Characterization of the Polymer Energy Landscape in Polymer:Fullerene Bulk Heterojunctions with Pure and Mixed Phases

Sean Sweetnam,[†] Kenneth R. Graham,[†,‡] Guy O. Ngongang Ndjawa,[‡] Thomas Heumüller,[†] Jonathan A. Bartelt,[†] Timothy M. Burke,[†] Wentao Li,[§] Wei You,[§] Aram Amassian,[‡] and Michael D. McGehee*,[†]

[†]Materials Science and Engineering Department, Stanford University, Stanford, California 94305-4034, United States

[‡]Materials Science and Engineering Program, Physical Sciences and Engineering Division, King Abdullah University of Science and Technology (KAUST), Thuwal, Saudi Arabia, 23955−6900

[§]Department of Chemistry, University of North Carolina at Chapel Hill, Chapel Hill, North Carolina 27599-3290, United States

Ⓢ Supporting Information

ABSTRACT: Theoretical and experimental studies suggest that energetic offsets between the charge transport energy levels in different morphological phases of polymer:fullerene bulk heterojunctions may improve charge separation and reduce recombination in polymer solar cells (PSCs). In this work, we use cyclic voltammetry, UV−vis absorption, and ultraviolet photoelectron spectroscopy to characterize hole energy levels in the polymer phases of polymer:fullerene bulk heterojunctions. We observe an energetic offset of up to 150 meV between amorphous and crystalline polymer due to bandgap widening associated primarily with changes in polymer conjugation length. We also observe an energetic offset of up to 350 meV associated with polymer:fullerene intermolecular interactions. The first effect has been widely observed, but the second effect is not always considered despite being larger in magnitude for some systems. These energy level shifts may play a major role in PSC performance and must be thoroughly characterized for a complete understanding of PSC function.
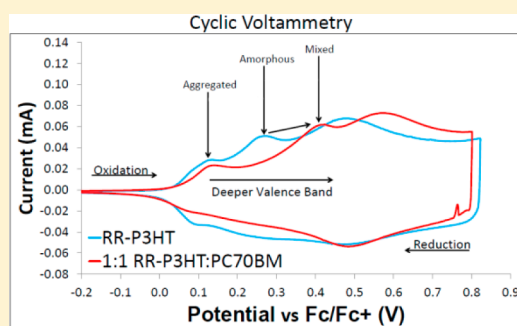
INTRODUCTION

The power conversion efficiency of bulk heterojunction (BHJ) polymer solar cells (PSCs) has increased substantially since the first use of an organic donor/acceptor interface to facilitate charge separation in an organic solar cell,[1] with device efficiencies now approaching 10%.[2] Increasing power conversion efficiencies beyond 10% requires a thorough understanding of the processes of charge carrier generation, separation, and collection in PSCs. Any successful model of these processes will need to account for the complex interplay between morphology and electronic structure inherent to BHJ PSCs.

An important morphological trend in BHJ PSCs containing fullerene derivative acceptor molecules has emerged, revealing that fullerene derivatives are miscible in disordered polymer phases up to 30% by weight at thermodynamic equilibrium.[3,4] However, the fullerene derivatives are not miscible in highly ordered (i.e., aggregated) polymer domains[5] with a few exceptions.[6,7] It has also been found that high-efficiency solar cells typically require polymer:fullerene blend ratios with weight fractions of fullerene beyond the fullerene miscibility limit in the disordered polymer,[8,9] resulting in the formation of fullerene-rich domains. These findings describe a morphological paradigm for high-efficiency PSCs consisting of at least three phases: a polymer-rich domain; a disordered domain composed of intimately mixed amorphous polymer and fullerene derivative; and a fullerene-rich domain.

Several groups have begun to connect the previously mentioned three-phase morphology with charge transport and generation in BHJ PSCs. Jamieson et al.[10] and Shoaee et al.[11] have proposed that energy cascades between disordered and ordered/aggregated domains improve geminate pair splitting in solar cells. Groves[12] and Burke[13] have used kinetic Monte Carlo simulations to show that an energy cascade between donor species in the mixed donor:acceptor phase and donor species in the pure donor phase can assist charge carrier extraction. These works suggest that understanding and characterizing the charge carrier energy levels of each donor and acceptor phase in a BHJ is crucial for our understanding of how charge carrier separation and extraction occurs in BHJ PSCs.

In this work the positions of the valence bands (VBs) of aggregated and amorphous polymer phases in BHJs of polymer:fullerene blends are measured using a combination of cyclic voltammetry (CV), in situ optical absorption spectroscopy, and ultraviolet photoelectron spectroscopy (UPS). CV is particularly useful in that it is a common

ACS Publications © 2014 American Chemical Society

14078

dx.doi.org/10.1021/ja505463r | J. Am. Chem. Soc. 2014, 136, 14078−14088

technique which is capable of measuring the energetic landscape of polymer:fullerene BHJs across multiple morphological phases. Two factors are found to affect the polymer VB in a polymer:fullerene BHJ.

First, in the case of semicrystalline polymer systems, variations in local polymer disorder create variations in the local polymer bandgap which is primarily due to changes in the conjugation length. A disorder induced increase in bandgap corresponds to a deeper VB (Figure 1) of the polymer and
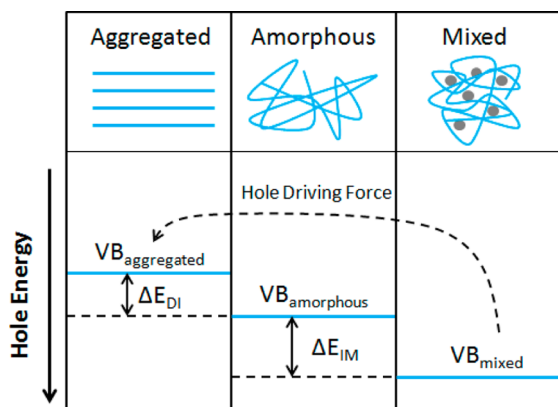

Figure 1. Energy level diagram depicting energetic offsets in the polymer VB caused by disorder-induced bandgap widening (ΔE_{DI}) and polymer:fullerene intermolecular interactions (ΔE_{IM}). The dashed arrow indicates the direction of the driving force for holes created by the energetic offsets in the polymer VBs.

results in an energetic offset, $\Delta E_{\text{Disorder Induced}}$ or ΔE_{DI}, between the VBs of well-ordered aggregated polymer domains and disordered amorphous polymer domains. The variation in bandgap across semicrystalline polymer phases has been commented on before[11,14] and is relatively well understood. We find values of ΔE_{DI} of up to 150 meV for several polymer systems.

Second, intermolecular interactions between the polymer and the fullerene derivative can also result in an energetic offset, $\Delta E_{\text{Intermolecular}}$ or ΔE_{IM} (Figure 1). This shift in the VB may result from charge transfer from the polymer to the fullerene

due to occupation of states in the electronic gaps of the organic materials[15−17] or from polarization of the molecules caused by electrostatic interactions between the polymer and fullerene such as induced dipole−induced dipole interactions or quadrupole−induced dipole interactions.[18−26] Although the energetic offset caused by intermolecular interactions has been characterized for some time by the UPS and computational modeling communities, it does not appear to be widely recognized within the PSC community. We find that the energetic offsets induced by polymer:fullerene intermolecular interactions appear to be general to polymer:fullerene blends, occurring in all polymer:fullerene blends studied here. These energetic offsets are also large in magnitude, ranging from 110 to 360 meV, making them as large as, and in some cases larger than, the energetic offsets caused by disorder-induced bandgap widening. These intermolecular interactions should therefore be recognized and understood by the PSC community to properly evaluate the energetic landscape of PSCs.

These energetic offsets between morphological phases likely have important implications for PSCs. The energetic offsets observed make it favorable for holes to move out of the polymer:fullerene mixed phase and into the pure polymer phase (Figure 1).[14] Holes are thus pushed out of phases with high concentrations of electrons (i.e., phases with higher fullerene concentration) and into phases with lower concentrations of electrons (i.e., polymer-rich phases), reducing recombination and increasing charge separation and extraction. We measure total energetic offsets between polymer phases on the order of 300 meV, which is predicted to have a large beneficial influence on charge separation.[12,13]

■ RESULTS AND DISCUSSION

Comparison of CV and UPS for Characterizing Polymer Valence Bands. There are a number of techniques that can characterize the VB of a material; in this work the polymer VB is characterized using CV and UPS.

CV is useful for characterizing the VB in polymers because it can characterize bulk material properties and can distinguish the VB of multiple polymer phases (i.e., aggregated and amorphous). Because CV requires penetration of ionic species and solvent molecules into the bulk of the polymer film, CV
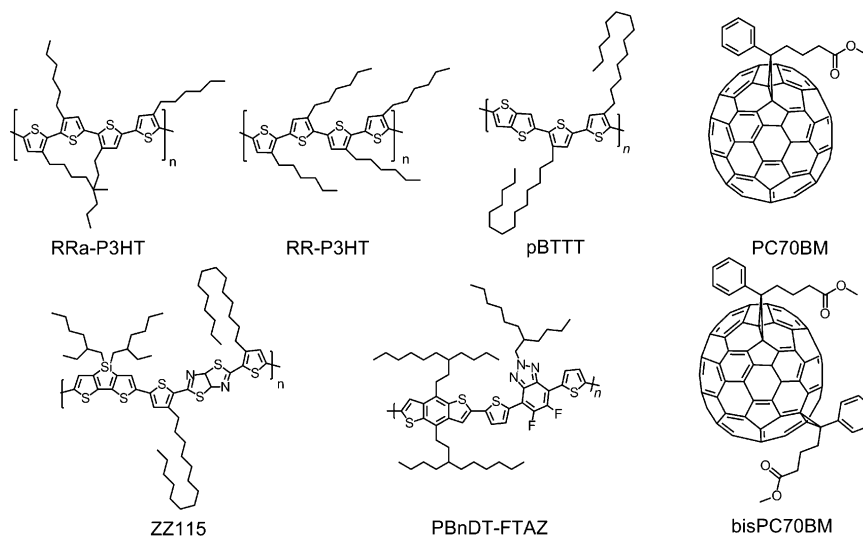

Figure 2. Molecular structure of polymers and fullerene derivatives studied in this work.

may alter the film morphology and energetics, creating uncertainty as to how the measured VB relates to the VB of the material in the absence of solvent and electrolyte. Note that although CV does not directly measure the absolute VB edge, this work is ultimately concerned with the relative position of the VBs of different polymer phases. CV allows for the determination of the relative oxidation potentials of the polymer phases, which also determine the relative positions of the polymer VBs.

UPS can also characterize the VB of polymers and does not involve any modification of the film morphology during measurement assuming no sample damage occurs.[27] UPS is surface sensitive, typically probing only the top few nm of a sample, and this surface sensitivity proves to be both an advantage and a disadvantage. UPS is useful for characterizing interface effects occurring only at the surface of a sample, and in particular bilayer morphologies can be used to perform careful studies of molecular interfaces. However, UPS is unable to easily probe bulk properties, and attempts to measure the bulk properties of polymer:fullerene blends with UPS may be hindered by vertical concentration gradients, e.g., polymer skin layers on the film surface.[28−30] In addition, though UPS is able to accurately determine the lowest binding energy VB of the aggregated polymer, it is unable to easily distinguish the amorphous polymer VB which is located at higher binding energies and is thus hidden under the density of states of the aggregated polymer.

We ultimately find CV to be most useful for characterizing the VB of all polymer phases in a BHJ polymer:fullerene film, as CV can distinguish both the aggregated and amorphous polymer oxidation processes. In this work we use UPS as a complementary technique, taking advantage of the surface sensitivity of UPS to probe the polymer:fullerene interface by monitoring changes in UPS spectra upon deposition of C60 onto a pure polymer film.

Energy Level Quantification of P3HT-Based BHJ. We begin by characterizing the VBs of pure regioregular (RR) poly(3-hexylthiophene-2,5-diyl) (P3HT) and a blend of RR-P3HT with [6,6]-phenyl C71 butyric acid methyl ester (PC70BM) (Figure 2). RR-P3HT is one of the most studied and best understood polymer systems for PSC applications, and PCBM is the most common acceptor material used in BHJ PSCs. The RR-P3HT:PCBM BHJ also exhibits the three-phase morphology present in many high-efficiency BHJ PSCs. These materials serve as good starting points for considering the VB of semicrystalline polymers in BHJ PSCs.

First consider the CV response of a pure RR-P3HT film (Figure 3a). Three oxidation peaks are observed on the forward scan. The first oxidation peak is attributed to the aggregated RR-P3HT, which is expected to be the most ordered polymer phase and therefore has the smallest bandgap, the VB closest to the Fermi level, and the smallest oxidation potential. The second and third oxidation peaks are attributed to amorphous RR-P3HT. We will confirm the assignment of these peaks later in this work.

One method of determining the position of the VB is to calculate the formal potential of a redox process by taking the average of the peak centers of the oxidation and reduction peaks. However, the reduction features observed in the samples presented in this work tend to be broad and overlapping, making it difficult to assign a peak position to the reduction process and thus difficult to assign the redox process a formal potential. Another method of assigning potentials to oxidation
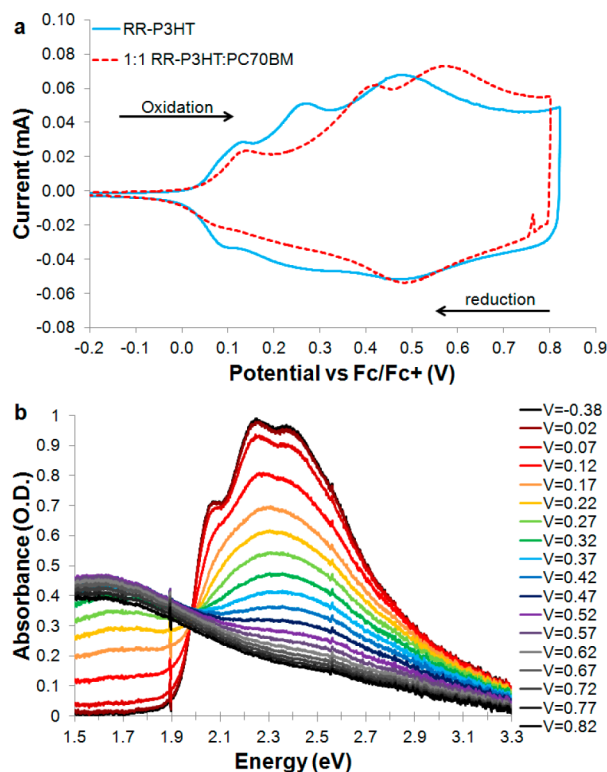

Figure 3. (a) CV measurements of thin films of pure RR-P3HT (blue, solid) and 1:1 RR-P3HT:PC70BM (red, dashed). Arrows indicate oxidation occurring during the forward scan of the sample (positive current) and reduction occurring during the reverse scan of the oxidized sample (negative current). (b) In situ optical absorption measurements obtained during the CV oxidation scan of the pure RR-P3HT sample shown in (a). The legend indicates the applied potential during the optical absorption measurement, from −0.38 V (top curve with maximum absorption of ∼ OD 1, near 2.25 eV) to 0.82 V (bottom curve with maximum optical density ∼ OD 0.4 near 1.5 eV).

processes is to estimate the onset of oxidation as the intersection of a linear background fit with a linear fit of the onset region of an oxidation peak. However, in the samples presented in this work the overlapping nature of the oxidation processes makes assignment of a linear onset of oxidation difficult. In this work the oxidation potential and VB are quantified as the peak of oxidation current for each oxidation process, as these peak values are well separated and more easily distinguished. Thus, in this work the analysis discusses only the oxidation features of the samples. Because the shape and position of oxidation features can depend on the CV scan rate, all CV scans were performed at the same slow scan rate of 10 mV/s. The oxidation peak positions of all samples studied in this work are summarized in Table S2 in the Supporting Information (SI). Having established our methodology for assigning oxidation potentials, the position of the oxidation peaks in the pure polymer film can be used to estimate the disorder induced energetic offset, ΔE_{DI}, between the aggregated and amorphous polymer VBs. ΔE_{DI} is calculated by measuring the peak-to-peak separation of the aggregated RR-P3HT (first oxidation peak) and the amorphous RR-P3HT (second oxidation peak), resulting in a measured ΔE_{DI} of 150 meV for RR-P3HT. All energetic offsets measured in this work are summarized in Table 1.

Next, the impact of polymer:fullerene mixing on the polymer VB is probed by performing CV on a thin film 1:1

Table 1. Energetic Offsets in the Polymer VB Induced by Polymer Disorder (ΔE_{DI}) and Polymer:Fullerene Intermolecular Interactions (ΔE_{IM})

polymer	$\Delta E_{DI}{}^{a}$ (meV)	ΔE_{IM} from CV^{b} (meV)	ΔE_{IM} from UPS^{c} (meV)
RR-P3HT	150	110–140	200
RRa-P3HT	N/A	170–360	230
pBTTT	N/A	240–320	340
pBnDT-FTAZ	130	120	110
ZZ115	N/A	N/A	130

$^{a}\Delta E_{DI}$ was estimated as the peak-to-peak separation of aggregated and amorphous polymer oxidation peaks obtained from CV. $^{b}\Delta E_{IM}$ determined by CV was estimated as the change in position of the polymer oxidation peaks after addition of PCBM, with a range of values listed when multiple peaks had changed position by different amounts. $^{c}\Delta E_{IM}$ determined by UPS was estimated by measuring the change in position of the polymer VB edge relative to the Fermi level after 10 Å C60 was evaporated onto the polymer.

weight:weight (wt:wt) RR-P3HT:PC70BM blend (Figure 3a). As in pure RR-P3HT there are three oxidation peaks. The addition of PC70BM to RR-P3HT has little impact on the first oxidation peak associated with the aggregated polymer. However, addition of PC70BM causes a dramatic change in the second and third oxidation peaks associated with the amorphous fraction of RR-P3HT, shifting them to higher potentials by 140 and 110 meV, respectively. It has been shown that PCBM is miscible with the amorphous fraction of RR-P3HT but does not mix with aggregated P3HT,[3,5,31−35] which suggests mixing of amorphous RR-P3HT with PC70BM results in the observed energetic offsets. The observed energetic offset, ΔE_{IM}, caused by addition of PC70BM is thus attributed to an intermolecular interaction between the polymer and the fullerene. We note that while one component of the energetic offset due to polymer:fullerene intermolecular interactions could be due to increased disorder in the amorphous polymer due to the presence of PCBM, an additional component due to electrostatic or electronic interactions between the polymer and fullerene is also needed to explain the observed energetic offsets.[17,20,22,24−26,36,37] We elaborate on this in the next section studying pBTTT.

Considered together, the energetic offsets due to polymer disorder and due to the polymer:fullerene intermolecular interaction result in a VB offset of almost 300 meV between the aggregated RR-P3HT and the amorphous RR-P3HT in the mixed region of a RR-P3HT:PC70BM blend. This energetic offset likely drives holes out of the deeper VB of the mixed amorphous polymer:fullerene phase and into the shallower VB of the aggregated pure polymer phase. We note that the magnitude of the energetic offsets observed throughout this work, ranging from 100 to 350 meV, are consistent with the energetic offsets predicted by computational modeling of polymer disorder and the donor:acceptor intermolecular interaction.[38,39]

To isolate the intermolecular interaction between amorphous P3HT and PCBM, CV was performed on regiorandom (RRa) P3HT, a completely amorphous P3HT isomer (Figure 2). Figure 4 shows the CV measurements of thin films of pure RRa-P3HT and 1:1 wt:wt RRa-P3HT:PC70BM. The addition of PC70BM to RRa-P3HT causes a dramatic change in the CV curve of the polymer, shifting the oxidation processes to higher potentials. This oxidation peak shift is independent of CV scan rate (Table S4), indicating the change is not due to kinetic
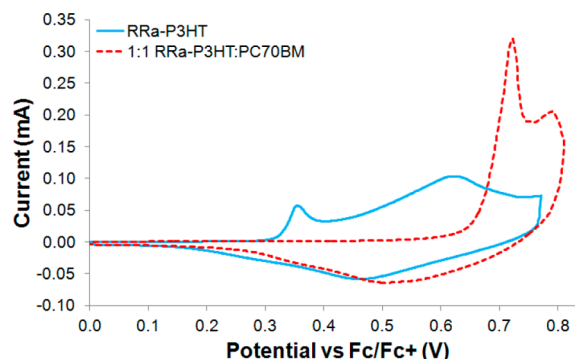

Figure 4. CV measurements of thin films of pure RRa-P3HT (blue, solid) and 1:1 RRa-P3HT:PC70BM (red, dashed).

limitations of electrochemical characterization (i.e., inhibited ion diffusion) but is instead due to some interaction between the polymer and fullerene. We find ΔE_{IM} between the RRa-P3HT and PC70BM to be between 170 meV (shift of second peak) to 360 meV (shift of first peak), which is larger than the ΔE_{IM} of 110−140 meV observed in RR-P3HT:PC70BM. It is beyond the scope of this study to conclusively state the cause for this increase in ΔE_{IM} for RRa-P3HT relative to RR-P3HT. However, we hypothesize that torsional defects in the RRa-P3HT may permit better mixing between RRa-P3HT and the fullerene. The torsional defects create a completely amorphous polymer with more free volume, allowing the polymer backbone to rotate and bend to make better contact with the fullerene. This better contact could take the form of a smaller polymer:fullerene separation, creating a stronger intermolecular interaction and thus larger energetic offset, or the form of a larger fraction of polymer monomers interacting with fullerenes, resulting in a larger energetic offset due to a larger number of interaction sites per polymer chain segment.

To confirm the assignment of the first (second/third) oxidation peak to the aggregated (amorphous) RR-P3HT, in situ optical absorption measurements (Figure 3b) were obtained during the CV measurement of the thin film RR-P3HT sample. At the initial potential of −0.38 V a typical absorption spectrum for a well-ordered RR-P3HT film is observed, with a bandgap of ~1.9 eV and several vibronic peaks that are associated with aggregated RR-P3HT domains.[40,41] There is little change in the absorption spectrum until the applied potential reaches 0.07 V, when the polymer begins to optically bleach simultaneously with the onset of polymer oxidation in the CV curve. This bleaching is most pronounced in the vibronic peaks, which suggests the oxidation occurs primarily in the polymer aggregates. The concurrence of the bleaching of the aggregated RR-P3HT absorption features with the first oxidation peak confirms that the first oxidation process is oxidation of the aggregated RR-P3HT. The aggregated RR-P3HT absorption features, i.e., the vibronic peaks, are completely bleached by 0.22 V. However, the second and third oxidation peaks occur at potentials higher than 0.22 V, indicating the second and third oxidation processes are not oxidation of aggregated RR-P3HT, and are therefore oxidation of amorphous RR-P3HT.

Another possibility that must be considered is that the second and third (amorphous polymer) oxidation peaks are additional oxidations (i.e., double and triple oxidations) of the oxidized aggregated polymer phase. However, several observations indicate it is unlikely that the second/third oxidation
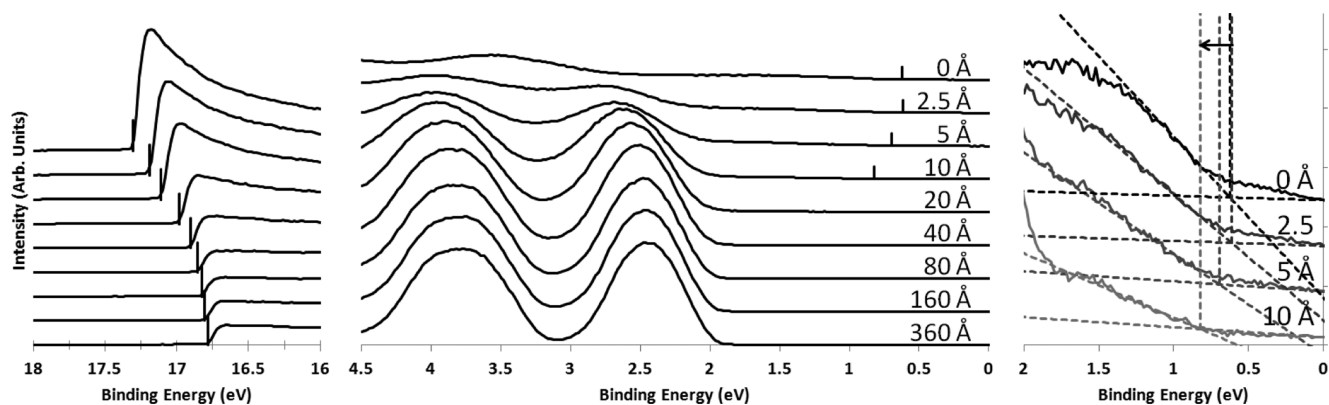
Figure 5. UPS spectra with He I excitation (21.22 eV) of RR-P3HT:C60 bilayer with stepwise evaporation of C60, from 0 Å C60 (top spectrum) to 360 Å C60 (bottom spectrum). Left: Secondary electron cutoff region with tick marks indicating position of cutoff. Middle: Onset region with tick marks indicating position of polymer VB edge. Fermi level is at 0 eV. Right: Zoomed-in view of onset region showing linear onset determination of polymer VB edge. Dashed lines show linear fits used to determine onset values, and arrow indicates change in position of onset as C60 thickness increases.

peaks are additional oxidations of the aggregated polymer but are instead oxidation processes of separate amorphous polymer phases. In brief, because the first oxidation peak is unaffected by addition of PCBM, we would not expect the second/third oxidation peaks to be affected by the addition of PCBM if they were additional oxidations of the aggregated polymer. Because the second/third oxidation peaks do change when PCBM is added, they are most likely not oxidation processes of the aggregated polymer. In addition, there is a strong resemblance between the second/third oxidation peaks of RR-P3HT and the oxidation peaks of the purely amorphous RRa-P3HT. This resemblance suggests the second/third oxidation peaks are most likely oxidation of amorphous P3HT, not additional oxidations of aggregated RR-P3HT. See Section B of the SI for additional discussion of this topic.

To further probe the intermolecular interaction at the RR-P3HT:fullerene molecular interface, UPS measurements are performed on RR-P3HT:C60 bilayers. In these measurements the UPS spectrum of a pure polymer film is recorded. Then a thin layer of C60 is deposited onto the polymer film, without removing the sample from ultra high vacuum, and the UPS spectrum is recorded again at the same spot on the sample. This process is iterated, sequentially depositing more C60 onto the sample and recording the UPS spectrum afterward. This process allows for comparison of the polymer VB in the absence and presence of fullerene. The sequential UPS spectra for the RR-P3HT:C60 bilayer are shown in Figure 5. We focus our analysis on the VB edge region of the UPS spectra (right panel in Figure 5), as this is the parameter relevant for hole transport in the polymer as it characterizes the position of the VB relative to the Fermi level.

As the C60 coverage increases from 0 to 10 Å, the RR-P3HT VB edge shifts further away from the Fermi level by 200 meV (right panel in Figure 5). This change in the VB is qualitatively consistent with the increased polymer oxidation potential observed in CV measurements of the RR-P3HT:PC70BM blends. Note that the polymer VB edge position is only quantified for C60 thicknesses up to 10 Å, as attenuation of the polymer signal for larger C60 thicknesses makes estimation of the polymer VB edge unreliable. From these UPS measurements ΔE_{IM} for RR-P3HT:C60 is estimated to be 200 meV. The same measurement is performed on a RRa-P3HT:C60 bilayer which yields a ΔE_{IM} of 230 meV (see Figure S5). The

results for ΔE_{IM} as determined by UPS are summarized in Table 1. The ΔE_{IM} predicted by UPS is quantitatively different from the ΔE_{IM} observed in CV. However, it is reasonable to expect there to be some quantitative difference in the ΔE_{IM} predicted by CV measurements of spin-cast polymer:PCBM blends and UPS measurements of polymer:C60 bilayers due to differences in sample morphology and molecular structure. The overall trend of a deeper polymer VB at the polymer:fullerene interface is consistent across both techniques.

When considering UPS spectra of organic systems, it is important to address some issues of experimental concern. When performing UPS on polymer samples it is possible that the UV light source can damage the sample. We see evidence of some sample damage in our measurements, specifically the presence of a weak density of states from 0 to 1 eV in the onset region (far right panel) of Figure 5. We attribute this weak density of states to defect states resulting from slight UV-induced sample damage. This signal is not related to the density of states of the polymer in a solar cell device, and thus we do not consider it when determining the position of the polymer VB. However, because sample damage is occurring, we must take precautions to ensure our measurements are accurate. Though we only report values for one scan on a sample in our analysis, multiple spots on each sample were measured, and each spot was scanned multiple times for each measurement to verify sample stability. We find for the systems studied here that the values measured on a given spot and scan are consistent with other spots and scans with a variance of <50 meV. For a comparison of onset and cutoff values obtained from different sample spots and scans see Table S8.

In addition, gap states can play a role in the energy level alignment at organic heterointerfaces, as previously mentioned.[16] Thus, the presence of damage-induced gap states in the UPS measurements may impact the energetic shift that occurs upon addition of C60. Because the CV measurements of P3HT samples demonstrate energy level shifts upon addition of PCBM despite the absence of exposure to a UV light source, we believe that the energetic offsets due to intermolecular interactions are present even in damage free samples and that our UPS analysis is in qualitative agreement with the CV analysis. However, due to the unknown quantitative impact of the presence of damage-induced gap states on energy level alignment, in addition to the differences in experimental

14082

dx.doi.org/10.1021/ja505463r | J. Am. Chem. Soc. 2014, 136, 14078–14088

conditions between CV and UPS, direct quantitative comparison between the energetic offsets predicted by CV and UPS cannot be made.

Energy Level Quantification of pBTTT BHJs. To determine if polymer:fullerene mixing leads to modification of the VB in polymer systems other than P3HT, we examine BHJs based on the polymer poly(2,5-bis(3-tetradecylthiophene-2-yl)thieno[3,2-*b*]thiophene) (pBTTT,[42] Figure 2). PC70BM is capable of intercalating between the side chains of pBTTT in the aggregated polymer phase,[6] and we have previously determined the crystal structure of the pBTTT:PC70BM bimolecular crystal,[43] thus pBTTT:PC70BM is a well-characterized model system in which only a mixed polymer:-fullerene phase is present. We have also shown that bisPC70BM (Figure 2) is not capable of intercalating between the pBTTT side chains due to steric hindrance from bisPC70BM's multiple solubilizing groups,[7] and thus no mixing between aggregated pBTTT and bisPC70BM occurs. By studying these two pBTTT blends, one with complete polymer:fullerene mixing in the aggregated phase and the other with no polymer:fullerene mixing in the aggregated phase, it is possible to further probe the impact of polymer:fullerene mixing on the polymer VB. The impact of pBTTT:fullerene mixing is probed by comparing thin film CV measurements of pure pBTTT with blends of 4:6 wt:wt pBTTT:PC70BM and pBTTT:bisPC70BM (Figure 6a). Pure pBTTT displays three closely spaced overlapping oxidation
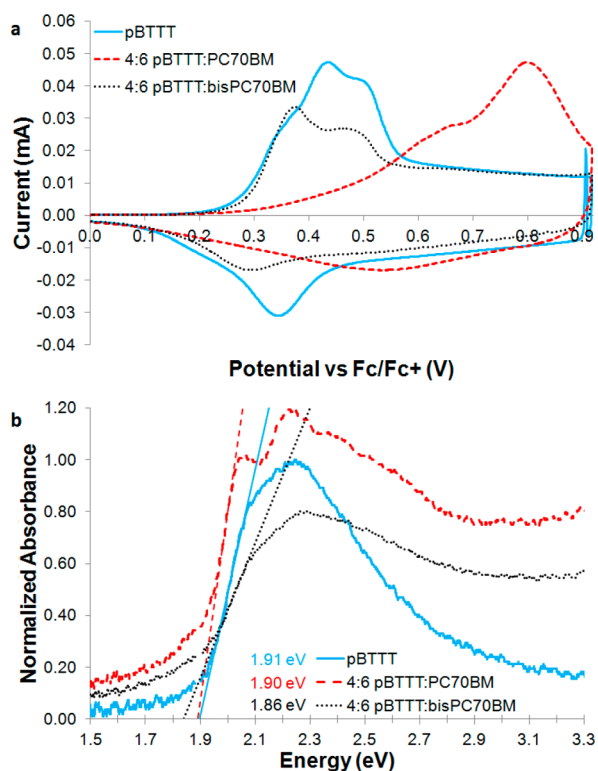
peaks. Addition of PC70BM to pBTTT substantially alters the CV response of the polymer, broadening the peaks and shifting them to higher potentials, with the first, second, and third oxidation peak potentials increasing by 250, 240, and 320 mV, respectively. Addition of bisPC70BM, however, has relatively little impact on the pBTTT oxidation features, with the oxidation peaks located in the same potential range as they are in pure pBTTT.

The CV measurements of pBTTT and pBTTT blends show that the addition of PC70BM to pBTTT results in a large ΔE_{IM} of up to 320 meV, while the addition of bisPC70BM does not strongly affect the position of the polymer oxidation features. These results again indicate that molecular mixing between the polymer and fullerene is accompanied by a powerful intermolecular interaction that modifies the polymer VB. When significant molecular mixing is absent, as in the case of pBTTT:bisPC70BM, the polymer VB is relatively unchanged.

To see if the shift in the pBTTT oxidation peaks caused by addition of PC70BM could be explained by disruption of pBTTT packing due to intercalation of PC70BM, the absorption spectra of the three pBTTT blends (Figure 6b) is measured. The optical absorption edge of all three samples is nearly identical, meaning no substantial change in polymer bandgap occurs upon addition of PC70BM or bisPC70BM. Moreover, the relatively weak and broad vibronic features observed in the pure pBTTT absorption spectrum become narrower and more pronounced upon addition of PC70BM, suggesting the PC70BM causes the pBTTT to become more ordered, not less ordered. This is consistent with Raman spectroscopy studies of pBTTT:PCBM which showed improved ordering in the pBTTT:PCBM bimolecular crystal compared to pure pBTTT.[44] Because pBTTT disorder may actually decrease in the presence of PC70BM, a mechanism other than disorder-induced bandgap widening must be responsible for the large increase in the oxidation potential of the pBTTT upon addition of PC70BM. Following the models proposed by the computational modeling and UPS communities, we hypothesize that a specific electronic interaction is responsible for the observed energetic offset.[17,20,22,24-26,36,37]

As in the case of P3HT, the pBTTT:fullerene molecular interface can be investigated by performing UPS measurements on pBTTT:C60 bilayers. This characterization is performed in the same manner as described previously for the RR-P3HT:C60 bilayers. As in the RR-P3HT:C60 bilayers, the pBTTT VB edge is shifted away from the Fermi level when C60 is deposited onto the polymer, in this case yielding a ΔE_{IM} of 340 meV. The presence of this intermolecular interaction between the polymer and fullerene in both P3HT and pBTTT suggests the effect may be general to many polymer:fullerene systems.

Energy Level Quantification of ZZ115 and PBnDT-FTAZ BHJs. The donor–acceptor polymers PBnDT-FTAZ[45] and poly[(4,4′-bis(2-ethylhexyl)dithieno[3,2-*b*:2′,3′-*d*]silole)-2,6-diyl-*alt*-(2,5-bis3-tetradecylthiophen-2-yl thiazolo 5,4-d thiazole)-2,5diyl] (ZZ115 or KP115[46]) operate relatively well in devices with large film thicknesses, with PBnDT-FTAZ (ZZ115) displaying 5.6% (4%) PCE in devices with 1000 (400) nm thick films. The relatively high performance in thick devices suggests the charge separation and collection processes are efficient in these polymers. If energetic offsets play a role in charge separation and collection in PSCs, then we expect these polymers to have large energetic offsets between the pure

Figure 6. (a) CV measurements of thin films of pure pBTTT (blue, solid), 4:6 wt:wt pBTTT:PC70BM (red, dashed) and 4:6 wt:wt pBTTT:bisPC70BM (black, dotted). (b) Scaled absorption spectra of thin films of pBTTT (blue, solid), 4:6 pBTTT:PC70BM (red, dashed) and 4:6 pBTTT:bisPC70BM (black, dotted). Linear extrapolations of absorption edges are indicated with colored lines and are used to estimate polymer bandgap in each film. Bandgap estimates are listed next to the figure legend.

aggregated polymer phase and the mixed amorphous polymer:-fullerene phase.

The characterization of PBnDT-FTAZ by CV, optical absorption, and UPS is comparable to those of RR-P3HT, RRa-P3HT, and pBTTT, and for brevity we have put the detailed analysis of this system in the SI. In brief, CV of pure pBnDT-FTAZ displays two distinguishable oxidation peaks that correspond to an aggregated and amorphous polymer phase. From these peaks we determine ΔE_{DI} to be 130 meV. Addition of [6,6]-phenyl C61 butyric acid methyl ester (PC60BM) shifts the second, amorphous oxidation peak to a higher potential, yielding a ΔE_{IM} of 120 meV. UPS measurements of PBnDT-FTAZ:C60 bilayers indicate the PBnDT-FTAZ VB shifts away from the Fermi level upon addition of C60, yielding a second estimate of ΔE_{IM} to be 110 meV. These results are summarized in Table 1.

The energy level offsets observed in PBnDT-FTAZ are very similar to those observed for the P3HTs and pBTTT. There is a relatively large (100−150 meV) energetic offset between the amorphous and aggregated pBnDT-FTAZ. There is also a strong interaction between pBnDT-FTAZ and fullerenes, resulting in an additional energetic offset of ∼100 meV. These two energetic offsets yield a total energetic offset of ∼200−300 meV between the pure aggregated polymer and mixed amorphous polymer, similar to the energetic offset observed in RR-P3HT:PCBM.

We turn now to ZZ115. The CV response of a thin film of ZZ115 (Figure 7a) is substantially more difficult to interpret
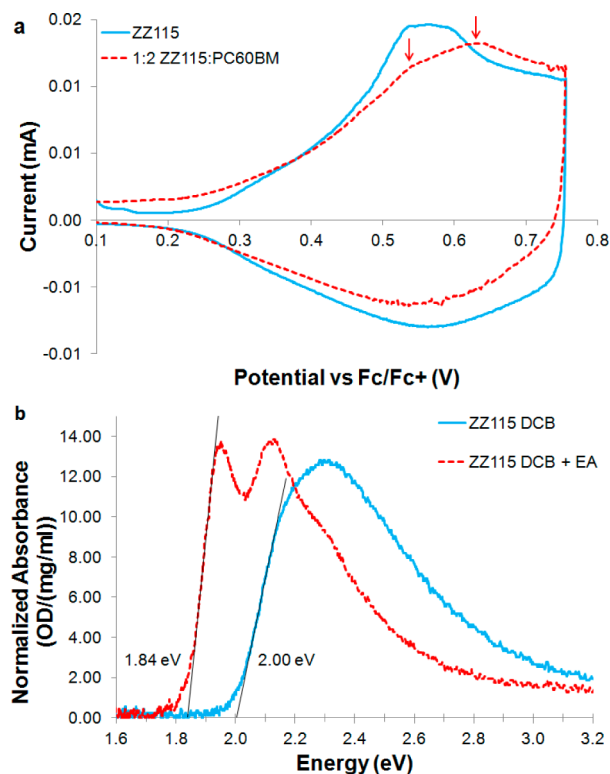
than that of the other polymer systems studied in this work. The CV response of RR-P3HT has three well-separated oxidation peaks, which allowed the assignment of the oxidation features to individual polymer phases with relative ease. In the case of ZZ115, however, there is a gradual onset of oxidation leading to a single broad oxidation feature, rather than several distinguishable oxidation peaks. Optical absorption spectra of the film (Figure S13) display vibronic peaks that suggest an aggregated polymer phase is present, and as such at least two oxidation peaks are expected in the CV response, one for aggregated polymer and one for amorphous polymer. Since two oxidation peaks are not observed, it is likely that the single broad oxidation peak is actually two broad overlapping oxidation peaks.

The CV curve of ZZ115 highlights one of the challenges of using CV to characterize the energetic landscape of polymers, namely that polymers often have large degrees of morphological disorder that lead to substantial energetic disorder.[47] This energetic disorder makes it difficult, in some cases prohibitively so, to use CV to characterize the energetic landscape of polymers. Optimization of sample preparation and measurement conditions can help to obtain separable oxidation peaks, with thinner samples and slower CV scan rates giving sharper oxidation features. However, in some cases the energetic disorder proves to be too large to allow quantification of oxidation peak positions using CV. For ZZ115, we are not able to quantitatively assign oxidation peak potentials for either the aggregated or amorphous polymer phases given the broad nature of the oxidation features.

Although we cannot quantitatively assign oxidation peak potentials for pure ZZ115, we can use complementary characterization techniques to estimate some of the properties of interest. For example, solution-state optical absorption can be used to estimate the upper limit of ΔE_{DI} by comparing the bandgap of aggregated and amorphous ZZ115. 1,2-dichlorobenzene (DCB) is a "good" solvent for ZZ115, and in solutions with low polymer concentrations (e.g., 20 μg/mL) ZZ115 is well dissolved with no aggregated polymer. Ethyl acetate (EA), on the other hand, is a "poor" solvent for ZZ115, causing ZZ115 to aggregate in solution when EA is added.[48] Figure 7b shows the solution-state absorption of ZZ115 in a well-dissolved state (140 °C in DCB) and an aggregated state (25 °C in a mixture of DCB and EA). The addition of EA induces a redshift in the absorption edge of the polymer and results in the emergence of several strong absorption peaks/shoulders. These changes in the absorption spectrum confirm that the polymer has aggregated in solution. The ZZ115 band-edge redshifts from 2.00 to 1.84 eV upon aggregation. From this shift, a maximum for ΔE_{DI} is estimated to be 160 meV. We note that although the change in VB position due to bandgap widening is often assumed to be half of the change in bandgap,[49] there is evidence that in some polymers the change in VB can be as large as the change in bandgap.[50] For this reason we do not assume the change in VB is equal to half the change in bandgap and instead use the solution-state absorption measurements to estimate the upper limit of the change in VB position.

The impact of blending fullerenes with ZZ115 is probed by measuring the CV response of a thin film of 1:2 wt:wt ZZ115:PC60BM (Figure 7a). The CV response of ZZ115:PC60BM has the same broad onset as the pure ZZ115 sample but displays two weak but distinguishable oxidation peaks rather than a single broad oxidation peak as was

Figure 7. (a) CV measurements of thin films of pure ZZ115 (blue solid) and 1:2 ZZ115:PC60BM (red dashed). Arrows indicate the position of the oxidation peaks in the 1:2 ZZ115:PC60BM blend. b) Solution state optical absorption of well-dissolved ZZ115 (blue solid line, in pure DCB at 140 °C) and aggregated ZZ115 (red dashed line, in DCB:EA at room temperature). Solution concentration was 20 μg/mL.

observed in the pure ZZ115. The presence of two oxidation peaks suggests there are two polymer phases, an aggregated and an amorphous phase, present in the film. This is consistent with the observation of aggregated polymer features (i.e., vibronic peaks) in absorption measurements of thin films of ZZ115 (Figure S13).

The first oxidation peak in the ZZ115:PC60Bm sample remains in approximately the same potential range as the beginning of the broad oxidation feature observed in pure ZZ115. We attribute this first peak to the aggregated polymer phase because it is located at a lower oxidation than the second peak, consistent with the idea that the aggregated polymer will be more ordered, have a smaller bandgap, and thus a VB closer to vacuum. We also attribute the first peak to aggregated polymer because its position does not change when PC60BM is added, consistent with the idea that PC60BM cannot mix with aggregated polymer phases, and thus does not change the position of the aggregated polymer oxidation peak. We attribute the second peak to the amorphous polymer phase using similar arguments to those just used, namely that the second oxidation peak occurs at higher potential and is thus the less ordered phase, and because its position changes when PC60BM is added and is thus mixing with the PC60BM. Although we cannot determine ΔE_{IM} from our CV measurements because we do not know the position of the amorphous polymer oxidation peak in the pure polymer, we can use the position of the two oxidation peaks in the ZZ115:PC60BM CV measurement to estimate the total energetic offset between the pure aggregated polymer phase and the mixed amorphous polymer:fullerene phase. We find the total energetic offset to be 90 meV. This is smaller than the energetic offsets observed in other systems, but still several times the thermal energy at room temperature, and thus likely to play a role in device performance.

To measure ΔE_{IM} between ZZ115 and the fullerene, the UPS spectra for ZZ115:C60 bilayers (Figure S14) are measured. As in RRa-P3HT, pBTTT, and PBnDT-FTAZ, deposition of C60 onto ZZ115 causes the VB to shift away from the Fermi level, yielding a ΔE_{IM} of 130 meV. This UPS determined ΔE_{IM} is larger than the total energetic offset estimated from CV, but as noted previously UPS and CV results are not expected to be quantitatively comparable. The general trend that addition of fullerene increases the oxidation potential of the polymer where it interacts/mixes is consistent across both techniques.

The energetic offsets observed in ZZ115 and PBnDT-FTAZ are qualitatively consistent with those observed in P3HT and pBTTT. There is a disorder-induced energetic offset between the VB of the aggregated and amorphous polymer fractions, as expected of semicrystalline polymers. There is also an energetic offset created by the polymer:fullerene intermolecular interaction. The total energetic offset between pure aggregated polymer and mixed amorphous polymer is ~200 and ~100 meV for PBnDT-FTAZ and ZZ115 respectively. These large energetic offsets in PBnDT-FTAZ and ZZ115 seem consistent with the hypothesis that large energetic offsets result in efficient charge extraction enabling devices optimizing with thick active layers.

Nature of the Intermolecular Interaction. The observation that all polymers studied in this work display a shift in VB when blended with fullerenes suggests the energetic offsets due to the polymer:fullerene interactions may be general to many, if not all, semiconducting-polymer:fullerene blends. It is also found that the magnitude of the polymer:fullerene intermo-

lecular interaction varies from polymer to polymer. For RRa-P3HT and pBTTT the observed ΔE_{IM} is in the range of 170–360 meV, whereas for RR-P3HT, ZZ115, and PBnDT-FTAZ the largest ΔE_{IM} observed is 140 meV. This difference in ΔE_{IM} for different polymer:fullerene blends suggests the polymer:fullerene intermolecular interaction depends on the particular polymer and fullerene being mixed. There may be some polymer:fullerene systems where ΔE_{IM} is small, and thus charge separation and collection is inefficient, which might explain why some seemingly promising polymer:fullerene blends perform below expectations.

The energetic offsets observed in this work are likely at play not only in the polymer but also the fullerene. It has already been shown that the energy levels of fullerenes change upon aggregation,[10] indicating a process similar to bandgap widening occurs in fullerenes as well as polymers. A brief examination of the UPS spectra of the RRa-P3HT:C60 bilayers in Figure 5 shows that the C60 density of states, two peaks between 2 and 4 eV, shifts toward the Fermi level as the thickness of C60 increases, indicating that the fullerene VB at the polymer:fullerene interface is different from the bulk fullerene VB. This change in the C60 VB would be consistent with a smaller bandgap due to C60 aggregation. It is also probable that the intermolecular interactions occurring at the polymer:fullerene interface affect the fullerene as well as the polymer. Computational models of donor:C60 intermolecular interactions predict large changes in the energy levels of both the donor and C60 at the heterointerface.[39] Although only the VB is measured by UPS and it is the conduction band (CB) that is relevant for electron transport in the fullerene, it is likely that changes in the fullerene VB due to polymer:fullerene intermolecular interactions or fullerene aggregation will be accompanied by changes in the C60 conduction band. Because we observe changes in the C60 VB in this work it is probable that the C60 CB changes as well, suggesting the types of energetic offsets observed in the polymer systems, ΔE_{DI} and ΔE_{IM}, play a role in fullerenes as well as in polymers, impacting charge transport and charge carrier recombination by determining where electrons reside in a PSC.

The mechanism of the polymer:fullerene intermolecular interaction is of particular interest. We would like to understand how these interactions influence material energetics to promote rational design of donor and acceptor materials, optimizing their chemical structures to tune the intermolecular interaction as appropriate for the application. It is beyond the scope of this work to determine the nature of the intermolecular interaction between the polymer and fullerene, but we will briefly mention two prominent models that may explain the observed intermolecular energy level shifts. These models have been developed within a theoretical and experimental framework for almost a decade, largely by the UPS and computational modeling communities, although these models and their importance may not be widely known within the broader PSC community.

One model describing the intermolecular interaction proposes charge transfer from the polymer to the fullerene occurs due to occupation of states in the electronic gaps of the organic materials,[15−17] resulting in band bending. This band bending could explain the observed shift of the polymer VB away from the Fermi level. Another model describes the intermolecular interaction in terms of polarization of the molecules due to electrostatic interactions between the polymer and fullerene.[18−26] In this model the donor energy levels are

modified by changes in the local environment due to induced dipole—induced dipole and quadrupole—induced dipole interactions, which could also explain the observed shift in the polymer VB. Both of these models seem plausible given the strong intermolecular interaction between the polymer and the fullerene as well as the observed change in VB, and it is possible that some component of the energy level shifts arises from electron transfer to or from gap states while another component arises from polarization effects. Both of these models also predict a change in the sample workfunction, measured by UPS, as C60 is evaporated onto the polymer, which is consistent with the secondary electron cutoff position changing as C60 is added (left panel of Figure 5). However, additional experimental verification, e.g., direct observation of ground-state charge transfer, is needed to determine which of these two models, or which aspects of them, are responsible for the observed energy level shifts.

CONCLUSION

We have characterized the hole transport levels across all polymer phases of several polymer:fullerene BHJs using a combination of CV, optical absorption, and UPS. We show that CV, a common technique found in most laboratories, is a particularly powerful tool for characterizing the energetic landscape across multiple phases of a polymer:fullerene BHJ. There are two primary factors that govern the energetic landscape for holes in polymers. First, differences in the degree of disorder between polymer domains (i.e., between aggregated and amorphous polymer domains) can result in energetic offsets due to bandgap widening of the polymer. Second, intermolecular interactions between the polymer and fullerene result in large changes in polymer energy levels. This second factor is often overlooked but may be quite important. While we observe at most a 150 meV energetic offset due to bandgap widening in the polymers studied, the intermolecular interactions between the polymer and fullerene can result in energy level shifts greater than 350 meV, indicating polymer:fullerene intermolecular interactions can alter the electronic properties of polymers as much as, or more than, changes in polymer ordering.

Furthermore, we believe energy level shifts due to intermolecular interactions should be general, applying not only to polymer:fullerene heterojunctions but to any organic donor:fullerene heterojunction. Any organic system that relies upon intermolecular electronic coupling for its function may be subject to the energetic offsets produced by intermolecular interactions, making the energetic offsets observed in this work relevant to organic photovoltaics as a whole.

Finally, the energetic offsets described in this work should play an important role in the function of a PSC. ΔE_{DI} destabilizes holes on the amorphous polymer, and ΔE_{IM} destabilizes holes in the mixed phase. Both of these effects push holes away from the mixed phase of amorphous polymer and fullerene, where electrons and holes are present in high concentrations, and toward the pure polymer phase, where there are relatively few electrons. By pushing holes away from electrons, these energetic offsets should work to reduce recombination, making them beneficial for PSC function.

EXPERIMENTAL SECTION

Spectroelectrochemical Samples and Measurements. Substrates used for electrochemical measurements were ITO-coated glass (Xinyan Technologies, Ltd.). Substrates were immersed in a detergent

solution of 1:9 extran:deionized water solution then scrubbed with a brush. Samples were then sonicated in the detergent solution, rinsed with deionized water, sonicated in acetone, sonicated in isopropanol, and blown dry with nitrogen. Substrates were stored in an oven held at 115 °C. Immediately before depositing films onto substrates, substrates were exposed to a UV-ozone plasma for 15 minutes.

PC70BM and PC60BM were purchased from Solenne BV. BisPC70BM was purchased from Nano-C. RR-P3HT (P200) was obtained from BASF. RRa-P3HT was obtained from Reike. Solutions of RR-P3HT, 1:1 wt:wt RR-P3HT:PC70BM, RRa-P3HT, and 1:1 RRa-P3HT:PC70BM were prepared in DCB at a polymer concentration of 25 mg/mL and were heated and stirred at 70 °C overnight. pBTTT was provided by the group of Martin Heeney. pBTTT, 4:6 wt:wt pBTTT:PC60BM, and 4:6 wt:wt pBTTT:bisPC70BM solutions were prepared in DCB at polymer concentrations of 5 mg/mL and were heated and stirred overnight at 70 °C. For pBTTT and PC70BM/bisPC70BM 4:6 wt:wt corresponds roughly to 1:1 molar:molar, the stoichiometry for pure bimolecular crystal in the case of pBTTT:PC70BM.[43] ZZ115 was provided by Konarka Technologies. ZZ115 and 1:2 wt:wt ZZ115:PC60BM solutions were prepared in DCB at polymer concentrations of 6.5 mg/mL and were heated and stirred overnight at 115 °C. PBnDT-FTAZ[45] was provided by the group of Wei You. PBnDT-FTAZ and 1:2 wt:wt PBnDT-FTAZ:PC60BM solutions were prepared in 1,2,4-trichlorobenzene (TCB) at polymer concentrations of 6 mg/mL and were heated and stirred overnight at 120 °C. All films were deposited in a nitrogen-filled glovebox (H2O and O2 levels typically <10 ppm) onto prepared substrates via spin-coating at 1000 rpm for 45 s with a ramp speed of 500 rpm/s. RR-P3HT, RRa-P3HT, pBTTT, and ZZ115 films and their blends were immediately placed into a covered Petri dish after spin-coating to allow them to dry slowly in a solvent-rich atmosphere. After spincasting, PBnDT-FTAZ films were quickly (within 5 min of spinning) put into a vacuum antechamber which was then evacuated in order to dry the films quickly. After drying and before being measured, RR-P3HT/RR-P3HT:PC70BM films were annealed at 110 °C for 10 min, and pBTTT/pBTTT:PC70BM/pBTTT:bisPC70BM films were annealed at 180 °C for 10 min.

CV measurements were performed on a Biologic VMP3 potentiostat. The electrolyte used was 0.02 M tetrabutylammonium hexafluorophosphate (TBA HFP) in acetonitrile. TBA HFP was purchased from Fluka. A platinum wire was used as a counter electrode, and a Ag/AgCl wire was used as a quasi-reference electrode. Nitrogen was bubbled through the electrolyte before each measurement to remove oxygen. All electrochemical measurements were performed at a scan rate of 10 mV/s. Ferrocene was used as a reference molecule. Our preferred method of determining the formal potential of ferrocene is as follows. After electrochemical measurement of a sample was performed, ferrocene was added to the electrolyte without removing the sample, and several CV curves of the sample were taken again in the ferrocene containing electrolyte. The formal potential of the ferrocene was determined from the CV curve containing both the ferrocene redox process and the sample redox process. However, for some samples it was difficult to determine the formal potential of the ferrocene when the sample was also present. In these cases, a blank substrate (cleaned patterned ITO-coated glass) was introduced, and the response of just the ferrocene was obtained. In general, we prefer not to use the first electrochemical cycle of our sample for our CV analysis. If no change was observed in the sample optical absorption spectrum after the first electrochemical cycle, then data from the first electrochemical cycle were not considered in our analysis. However, in some samples (in our case RRa-P3HT and pBTTT) irreversible changes occurred in the optical absorption spectrum after the first electrochemical cycle. In these systems, only the first electrochemical cycle was considered for our analysis. Optical absorption measurements were performed with an Ocean Optics USB4000 spectrometer and a Analytical Instrument systems Model DT 1000 CE UV−vis Lightsource. Absorption spectra were measured once every second during CV measurements. Absorption spectra were time averaged for 600 ms.

UPS Samples and Measurements. Substrates used for UPS measurements were poly(3,4-ethylenedioxythiophene) poly-(styrenesulfonate) (PEDOT:PSS, Clevios VP Al 4083) coated gold foils. The gold foil was cleaned through sonication in acetone followed by UV ozone exposure for 15 min. Following UV ozone exposure PEDOT:PSS was spincast at 5000 rpm for 40 s. PEDOT:PSS was annealed on a hot plate in air at 130 °C for 15 min prior to taking substrates into a nitrogen-filled glovebox (H_2O and O_2 typically <5 ppm) for casting of the polymer solutions. The same batches of polymer used for the CV measurements were used for the UPS measurements, with the exception of RR-P3HT UPS samples which were prepared with RR-P3HT from Sigma-Aldrich (item no. 445703). The RR-P3HT, RRa-P3HT, pBTTT, and ZZ115 solutions were prepared at 4 mg/mL in CB, and the PBnDT-FTAZ solution was prepared in DCB, and all solutions were stirred overnight at 100 °C. PBnDT-FTAZ and ZZ115 were spincast at 100 °C at 3000 rpm with a ramp speed of 3000 rpm/s for 45 s. pBTTT was spun at 100 °C and RRa-P3HT was spun at 60 °C, and pBTTT and RRa-P3HT were spincast at 2000 rpm with a ramp speed of 2000 rpm/s for 45 s. The resulting polymer film thicknesses were between 12 and 18 nm.

Following polymer film deposition the samples were transferred under HV conditions (1×10^{-6} mbar) from the glovebox to the UPS analysis/C60 evaporation chambers. UPS measurement and C60 evaporation occurred within the same UHV system (base pressure <1 $\times 10^{-9}$ mbar). The samples were thus never exposed to air. C60 (sublimed grade) was purchased from Sigma-Aldrich. The C60 was purified in ultrahigh vacuum (UHV) by heating the material at 350 °C for 8−24 hours after an initial 12−24 hours bakeout at 120 °C. UPS measurements were performed with a SPHERA electron energy analyzer with a He I, 21.22 eV, discharge source (Omicron), with pass energies of 2.5 and 1.8 eV (for valence region and secondary electron cutoff region, respectively) during stepwise deposition of C60. Multiple spots were initially analyzed on each sample, and the spots that yielded stability under repeated UPS scans were selected for analysis during the C60 deposition. During the stepwise deposition C60 was evaporated at a temperature of 440 °C and a typical rate of 3−5 Å/min. UPS spectra were recorded after each stepwise C60 deposition.

ASSOCIATED CONTENT

Ⓢ Supporting Information

Methods for determining the oxidation potentials using CV, complete list of the oxidation peak potentials considered in this work, and additional characterization of RR-P3HT, pBTTT, ZZ115, and PBnDT-FTAZ using CV, optical absorption, and UPS. This material is available free of charge via the Internet at http://pubs.acs.org.

AUTHOR INFORMATION

Corresponding Author
mmcgehee@stanford.edu
Notes
The authors declare no competing financial interest.

ACKNOWLEDGMENTS

REFERENCES

(1) Tang, C. W. *Appl. Phys. Lett.* **1986**, *48*, 183.
(2) Cruickshank, C. Toray develops polymer organic photovoltaic and acheives efficiency of 10.6% . *The OSADirect Newsletter*; cintelliq Limited: Cambridge, U.K.; http://www.osadirect.com/news/article/1055/ (accessed September 12, 2014).
(3) Collins, B. A.; Gann, E.; Guignard, L.; He, X.; McNeill, C. R.; Ade, H. *J. Phys. Chem. Lett.* **2010**, *1*, 3160.
(4) Collins, B. A.; Li, Z.; Tumbleston, J. R.; Gann, E.; McNeill, C. R.; Ade, H. *Adv. Energy Mater.* **2013**, *3*, 65.
(5) Treat, N. D.; Brady, M. A.; Smith, G.; Toney, M. F.; Kramer, E. J.; Hawker, C. J.; Chabinyc, M. L. *Adv. Energy Mater.* **2011**, *1*, 82.
(6) Mayer, A. C.; Toney, M. F.; Scully, S. R.; Rivnay, J.; Brabec, C. J.; Scharber, M.; Koppe, M.; Heeney, M.; McCulloch, I.; McGehee, M. D. *Adv. Funct. Mater.* **2009**, *19*, 1173.
(7) Miller, N. C.; Cho, E.; Gysel, R.; Risko, C.; Coropceanu, V.; Miller, C. E.; Sweetnam, S.; Sellinger, A.; Heeney, M.; McCulloch, I.; Brédas, J.-L.; Toney, M. F.; McGehee, M. D. *Adv. Energy Mater.* **2012**, *2*, 1208.
(8) Cates, N. C.; Gysel, R.; Beiley, Z.; Miller, C. E.; Toney, M. F.; Heeney, M.; McCulloch, I.; McGehee, M. D. *Nano Lett.* **2009**, *9*, 4153.
(9) Bartelt, J. A.; Beiley, Z. M.; Hoke, E. T.; Mateker, W. R.; Douglas, J. D.; Collins, B. A.; Tumbleston, J. R.; Graham, K. R.; Amassian, A.; Ade, H.; Fréchet, J. M. J.; Toney, M. F.; McGehee, M. D. *Adv. Energy Mater.* **2013**, *3*, 364.
(10) Jamieson, F. C.; Domingo, E. B.; McCarthy-Ward, T.; Heeney, M.; Stingelin, N.; Durrant, J. R. *Chem. Sci.* **2012**, *3*, 485.
(11) Shoaee, S.; Subramaniyan, S.; Xin, H.; Keiderling, C.; Tuladhar, P. S.; Jamieson, F.; Jenekhe, S. A.; Durrant, J. R. *Adv. Funct. Mater.* **2013**, *23*, 3286.
(12) Groves, C. *Energy Environ. Sci.* **2013**, *6*, 1546.
(13) Burke, T. M.; McGehee, M. D. *Adv. Mater.* **2014**, *26*, 1923.
(14) Noriega, R.; Rivnay, J.; Vandewal, K.; Koch, F. P. V; Stingelin, N.; Smith, P.; Toney, M. F.; Salleo, A. *Nat. Mater.* **2013**, *12*, 1038.
(15) Hwang, J.; Kim, E.; Liu, J.; Brédas, J.-L.; Duggal, A.; Kahn, A. *J. Phys. Chem. C* **2007**, *111*, 1378.
(16) Mao, H. Y.; Bussolotti, F.; Qi, D.-C.; Wang, R.; Kera, S.; Ueno, N.; Wee, A. T. S.; Chen, W. *Org. Electron.* **2011**, *12*, 534.
(17) Guerrero, A.; Marchesi, L. F.; Boix, P. P.; Ruiz-Raga, S.; Ripolles-Sanchis, T.; Garcia-Belmonte, G.; Bisquert, J. *ACS Nano* **2012**, *6*, 3453.
(18) Fukagawa, H.; Yamane, H.; Kera, S.; Okudaira, K.; Ueno, N. *Phys. Rev. B* **2006**, *73*, 041302.
(19) Duhm, S.; Heimel, G.; Salzmann, I.; Glowatzki, H.; Johnson, R. L.; Vollmer, A.; Rabe, J. P.; Koch, N. *Nat. Mater.* **2008**, *7*, 326.
(20) Verlaak, S.; Beljonne, D.; Cheyns, D.; Rolin, C.; Linares, M.; Castet, F.; Cornil, J.; Heremans, P. *Adv. Funct. Mater.* **2009**, *19*, 3809.
(21) Topham, B. J.; Kumar, M.; Soos, Z. G. *Chem. Phys. Lett.* **2010**, *493*, 251.
(22) Linares, M.; Beljonne, D.; Cornil, J.; Lancaster, K.; Brédas, J.-L.; Verlaak, S.; Mityashin, A.; Heremans, P.; Fuchs, A.; Lennartz, C.; Idé, J.; Méreau, R.; Aurel, P.; Ducasse, L.; Castet, F. *J. Phys. Chem. C* **2010**, *114*, 3215.
(23) Monti, O. L. A. *J. Phys. Chem. Lett.* **2012**, *3*, 2342.
(24) Mothy, S.; Guillaume, M.; Idé, J.; Castet, F.; Ducasse, L.; Cornil, J.; Beljonne, D. *J. Phys. Chem. Lett.* **2012**, *3*, 2374.
(25) D'Avino, G.; Mothy, S.; Muccioli, L.; Zannoni, C.; Wang, L.; Cornil, J.; Beljonne, D.; Castet, F. *J. Phys. Chem. C* **2013**, *117*, 12981.
(26) Ryno, S. M.; Risko, C.; Brédas, J.-L. *J. Am. Chem. Soc.* **2014**, *136*, 6421.

(27) Opitz, A.; Frisch, J.; Schlesinger, R.; Wilke, A.; Koch, N. *J. Electron Spectrosc. Relat. Phenom.* **2013**, *190*, 12.

(28) Hoppe, H.; Sariciftci, N. S. *J. Mater. Chem.* **2006**, *16*, 45.

(29) Guan, Z.-L.; Kim, J. B.; Wang, H.; Jaye, C.; Fischer, D. A.; Loo, Y.-L.; Kahn, A. *Org. Electron.* **2010**, *11*, 1779.

(30) Guan, Z.-L.; Bok Kim, J.; Loo, Y.-L.; Kahn, A. *J. Appl. Phys.* **2011**, *110*, 043719.

(31) Watts, B.; Belcher, W. J.; Thomsen, L.; Ade, H.; Dastoor, P. C. *Macromolecules* **2009**, *42*, 8392.

(32) Kiel, J. W.; Eberle, A. P. R.; Mackay, M. E. *Phys. Rev. Lett.* **2010**, *105*, 168701.

(33) Parnell, A. J.; Cadby, A. J.; Mykhaylyk, O. O.; Dunbar, A. D. F.; Hopkinson, P. E.; Donald, A. M.; Jones, R. A. L. *Macromolecules* **2011**, *44*, 6503.

(34) Kozub, D. R.; Vakhshouri, K.; Orme, L. M.; Wang, C.; Hexemer, A.; Gomez, E. D. *Macromolecules* **2011**, *44*, 5722.

(35) He, X.; Collins, B. A.; Watts, B.; Ade, H.; McNeill, C. R. *Small* **2012**, *8*, 1920.

(36) Osikowicz, W.; de Jong, M. P.; Salaneck, W. R. *Adv. Mater.* **2007**, *19*, 4213.

(37) Braun, S.; Salaneck, W. R.; Fahlman, M. *Adv. Mater.* **2009**, *21*, 1450.

(38) McMahon, D. P.; Cheung, D. L.; Troisi, A. *J. Phys. Chem. Lett.* **2011**, *2*, 2737.

(39) Cornil, J.; Verlaak, S.; Martinelli, N.; Mityashin, A.; Olivier, Y.; Van Regemorter, T.; D'Avino, G.; Muccioli, L.; Zannoni, C.; Castet, F.; Beljonne, D.; Heremans, P. *Acc. Chem. Res.* **2013**, *46*, 434.

(40) Spano, F. C. *J. Chem. Phys.* **2005**, *122*, 234701.

(41) Spano, F. C. *Chem. Phys.* **2006**, *325*, 22.

(42) McCulloch, I.; Heeney, M.; Bailey, C.; Genevicius, K.; Macdonald, I.; Shkunov, M.; Sparrowe, D.; Tierney, S.; Wagner, R.; Zhang, W.; Chabinyc, M. L.; Kline, R. J.; McGehee, M. D.; Toney, M. F. *Nat. Mater.* **2006**, *5*, 328.

(43) Miller, N. C.; Cho, E.; Junk, M. J. N.; Gysel, R.; Risko, C.; Kim, D.; Sweetnam, S.; Miller, C. E.; Richter, L. J.; Kline, R. J.; Heeney, M.; McCulloch, I.; Amassian, A.; Acevedo-Feliz, D.; Knox, C.; Hansen, M. R.; Dudenko, D.; Chmelka, B. F.; Toney, M. F.; Brédas, J.-L.; McGehee, M. D. *Adv. Mater.* **2012**, *24*, 6071.

(44) Gao, J.; Thomas, A. K.; Johnson, R.; Guo, H.; Grey, J. K. *Chem. Mater.* **2014**, *26*, 4395.

(45) Price, S. C.; Stuart, A. C.; Yang, L.; Zhou, H.; You, W. *J. Am. Chem. Soc.* **2011**, *133*, 4625.

(46) Peet, J.; Wen, L.; Byrne, P.; Rodman, S.; Forberich, K.; Shao, Y.; Drolet, N.; Gaudiana, R.; Dennler, G.; Waller, D. *Appl. Phys. Lett.* **2011**, *98*, 043301.

(47) Rivnay, J.; Noriega, R.; Northrup, J.; Kline, R.; Toney, M.; Salleo, A. *Phys. Rev. B* **2011**, *83*, 1.

(48) Scharsich, C.; Lohwasser, R. H.; Sommer, M.; Asawapirom, U.; Scherf, U.; Thelakkat, M.; Neher, D.; Köhler, A. *J. Polym. Sci., Part B: Polym. Phys.* **2012**, *50*, 442.

(49) Bredas, J. L.; Silbey, R.; Boudreaux, D. S.; Chance, R. R. *J. Am. Chem. Soc.* **1983**, *105*, 6555.

(50) Tsoi, W. C.; Spencer, S. J.; Yang, L.; Ballantyne, A. M.; Nicholson, P. G.; Turnbull, A.; Shard, A. G.; Murphy, C. E.; Bradley, D. D. C.; Nelson, J.; Kim, J.-S. *Macromolecules* **2011**, *44*, 2944.